DOI: 10.21062/mft.2025.039 http://www.journalmt.com

Thermal Analysis of Micro Plasma Wire Arc Additive Manufacturing Deposition Process

Siti Khairiyah Sulaiman (0009-0002-0734-516X)[1], Mohd Rizal Alkahari (0000-0001-7164-5859)[1,2], Mohd Juzaila Abd Latif (0000-0002-7880-985X)[1], Yupiter Harangan Prasada Manurung (0000-0003-3191-9944)[3,4], Keval Priapratama Prajadhiana (0000-0002-5578-7870)[3,4]
[1]Faculty of Mechanical Technology and Engineering, Universiti Teknikal Malaysia Melaka, 76100, Durian Tunggal, Melaka, Malaysia.
[2]Center for Advanced Research on Energy, Universiti Teknikal Malaysia Melaka, 76100, Durian Tunggal, Melaka, Malaysia. E-mail: rizalalkahari@utem.edu.my
[3]College of Engineering, Universiti Teknologi MARA, Shah Alam, Selangor, Malaysia.
[4]Smart Manufacturing Research Institute, Universiti Teknologi MARA, Shah Alam, Selangor, Malaysia.

Additive manufacturing (AM) is rapidly developing with emerging technology of wire arc additive manufacturing (WAAM) process due to its ability to manufacture large components and high deposition rate. However, WAAM faces mechanical properties problems like porosity, distortion, and strength due to the large heat affected zone (HAZ) from commonly used heat sources such as metal inert gas (MIG) and tungsten inert gas (TIG). Utilization of micro plasma as the heat source should reduce this problem since it has a smaller heat source diameter. Therefore, this study investigates the thermal distribution of micro plasma wire arc additive manufacturing (MPWAAM) by developing a finite element method (FEM) model. This paper focuses on the fabrication of single-layer multitrack deposition and tool path planning of multi-layer multitrack depositions by MPWAAM process. The melt pool size and peak temperature are mainly governed by heat input per unit travel speed of the worktable, with current and voltage being the significant factors. Besides, tool path planning strategy influences the properties and quality of the final product, where parallel tool path design with longer interlayer cooling time minimized part distortion and residual stresses.

Keywords: Additive Manufacturing, 3D Printing, Finite Element Method, Wire Arc Additive Manufacturing, Multi-layer multitrack

1 Introduction

Additive Manufacturing (AM) is a crucial technology in the context of the Industrial Revolution 4.0 (IR 4.0). and has high potential for the manufacturing of metal and non-metal parts. However, the lack of understanding on factors affecting the characteristics of the 3D printed structure has become a barrier to its wider adoption [1]. Metal AM is a complex process which include repetitive heating, cooling, solidification, and reheating during layer-by-layer fabrication. There are different types of metal additive manufacturing technique and one of them is wire arc additive manufacturing (WAAM). WAAM is a process that produces metallic parts by deposition of weld beads, melting, and solidifying layers of metal wire. There is a growing interest in WAAM, leading to substantial ongoing research activities. [2].

However, WAAM faces challenges such as poor dimensional accuracy, feature resolution, and surface finish, leading to tolerance loss. The high heat-affected zone of metal inert gas (MIG) and tungsten inert gas (TIG) heat sources and the high periodic heat input due to arc welding make controlling these issues challenging [3]. These problems lead to the proposal of using microplasma as the heat source during the WAAM process because it has smaller heat source dimensions and a plasma arc current of less than 30 A. The use of microplasma as the heat source can lessen this issue because it can deposit smaller components because it has a smaller heat source dimension and a narrower plasma arc heating zone than a TIG [4-7].

Previous research on AM has shown that varying combinations of process parameters can significantly improve part quality; a similar approach can be applied to WAAM using microplasma to enhance mechanical properties and dimensional accuracy [8]**.** The width and height of the deposition are directly related to the input power and the pace at which material is deposited [9]. The flow pattern inside the molten pool is influenced by the power of the heat source and the relative speed. Once the welding pool stabilises, numerical models may calculate these parameters [10].

Path planning in AM is of utmost importance since various path techniques have a direct impact on the surface roughness, dimensional accuracy, and strength

qualities of the printed goods. There are study on geometric accuracy that highlights the impact of model orientation during printing, which similarly underscores the importance of toolpath planning in multi-track WAAM, where deposition direction and sequence significantly affect dimensional precision and part integrity [11]. Varying trajectories necessitate distinct motion techniques for the print head, leading to varying production durations [12].

WAAM's deposition quality is linked to the tool path strategy used. This solution ensures uniform deposition by dividing layers into basic geometry, simplifying deposition prediction. Combining efficiency and adaptability, it offers a diverse material and deposition process. Users can intervene during the path generation, improving result quality and enabling local parameter changes [13]. Thus, this work aims to conduct 3D thermal analysis on the fabrication of single-track deposits with multiple scanning speed, current, and voltage combinations to understand their effect on the melt pool formation and peak temperature reached.

2 Methodology

In this study, Finite Element Method based numerical simulation is carried out using Simufact Welding 2022.0.1 to study the effects of heat input: speed, current and voltage. The WAAM setup utilised a direct energy deposition method, with a specific focus on thermal calibration where the analysis was limited to the thermal process.

2.1 Modelling

Micro-plasma arc heat source travels perpendicular to the substrate material deposited in the middle of the base plate. A consistent distance is maintained between the torch and the substrate material. The base plate is clamped on the bearing at two corners with a distance of 50 mm from the edges as shown in Fig. 1.

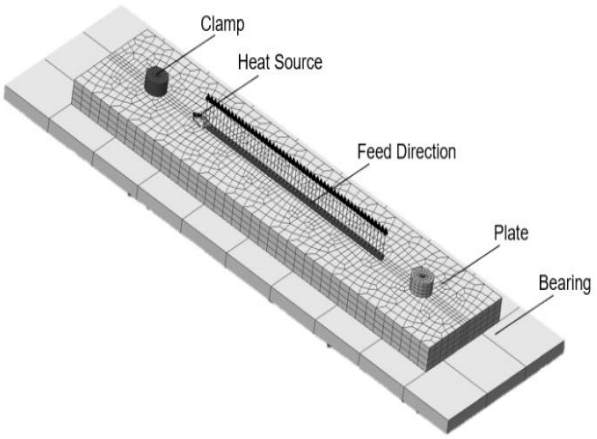

Fig. 1 *MPWAAM Model Setup*

For thermal analysis, the temperature-dependent properties of the material are essential for the accurate measurement of the temperature field. The thermal-mechanical features are isotropic and homogeneous throughout the heat assessment.

Material thermal features of both straight weld seam of Stainless Steel 316 with 100 mm length on base plate made by stainless steel 304 [14] are temperature dependent to determine the heat flux produced and time is taken for weld seam to build up and form first layer. As indicated in Tab. 1, distinct temperature conditions were used for the base plate and the weld seam, allowing for the application of various parameters to contact areas.

Tab. 1 *Thermal boundary conditions for FEM simulations*

Heat Transfer Coefficient		
To environment	Base to table	Base to weld
16W/m²K	225W/m²K	10000W/m²K

2.2 Heat Input Model

This study applied Goldak heat input model, which is a volumetric heat source specified in a moving frame of reference as a double-ellipsoidal [15]. Parameters of the heat input model which are heat deposited fractional factors in the rear and front quadrant characterised by four parameters: width (*a*), depth (*b*), front length (c_f) and rear length (c_r). The sum of these factors is equal to 2. Previous research studied on these heat input parameters and the influence on residual stress and distortion using FE model where they also validate the model with experimental results [10,16,17]. Detailed values for each dimensions is shown in Tab. 2 as referred from previous research that utilise plasma arc as the heat source [16].

Tab. 2 *Heat source dimension*

Heat Source Dimensions	**Value (mm)**
Width, (a)	2.5
Depth, (b)	4
Front Length, (c_f)	1.75
Rear Length, (c_r)	3

2.3 Processing Parameters

Melt pool formation in the WAAM process is affected by the heat input, which is influenced by the current, voltage, and travel speed. The relationship between welding parameters and heat input is shown in Equation (1) where value of K=1 here is for WAAM or arc welding as previous study [18]. And as expressed by Equation (2), heat input increases with pulse energy.

$$\text{Heat Input} = \frac{K \times V \times I \times 60}{S \times 1000} \quad (1)$$

Where:
V…Arc Voltage [Volts];
I…Welding Current [Ampere];
S…Welding Speed [mm/min];
K…Thermal Efficiency Factor [-].

$$\text{Heat Input} = \frac{E \times f}{V} \quad (2)$$

Where:
E…Pulse Energy;
f…Pulse Frequency;
V…Welding Speed [mm/min].

This study selects five levels of parameters for experiments, and an orthogonal array of L30 as shown in Tab. 3 is designed to investigate the effect of main factors and interaction effects. Random trial runs are conducted to avoid experimental setup influence during data collection [19].

Tab. 3 *Processing parameters with their levels*

Parameters	Units	Levels				
		L1	L2	L3	L4	L5
Speed	mm/s	32	34	36	38	40
Current	A	20	25	30	35	40
Voltage	V	16	18	20	22	24

2.4 Path Planning Strategies

Path planning aims to save materials or time and improve mechanical, topological, or functional properties, that ultimately enhancing the overall 3D printed properties [12]. This work study on influence of deposition direction on two different tool path plan as shown in Fig. 2 below; where Fig. 2 (a) shows parallel path and Fig. 2 (b) shows zigzag path which in back and forth movement.

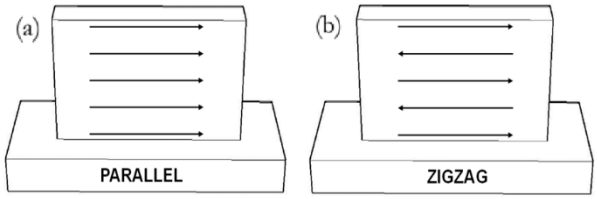

Fig. 2 *Tool path in (a) Parallel, (b) Zigzag direction*

After the deposition time period is completed, the micro-plasma arc travels to the next area and a continuous simulation occurs for the whole geometry of the deposition layer. Once the first layer of deposition has been simulated, the micro-plasma arc transitions to a new layer and the entire simulation process is repeated until a total of 20 layers have been deposited. The nodal temperature distribution for each deposition layer is recorded to monitor thermal distortion.

2.5 Validation of FE Model

Experimental validation was conducted using a pyrometer shown in Fig. 3 to monitor temperature during single track deposition. This FE model was verified by comparing the peak temperature on the experimental single track deposition and the peak temperature generated from the FE model.

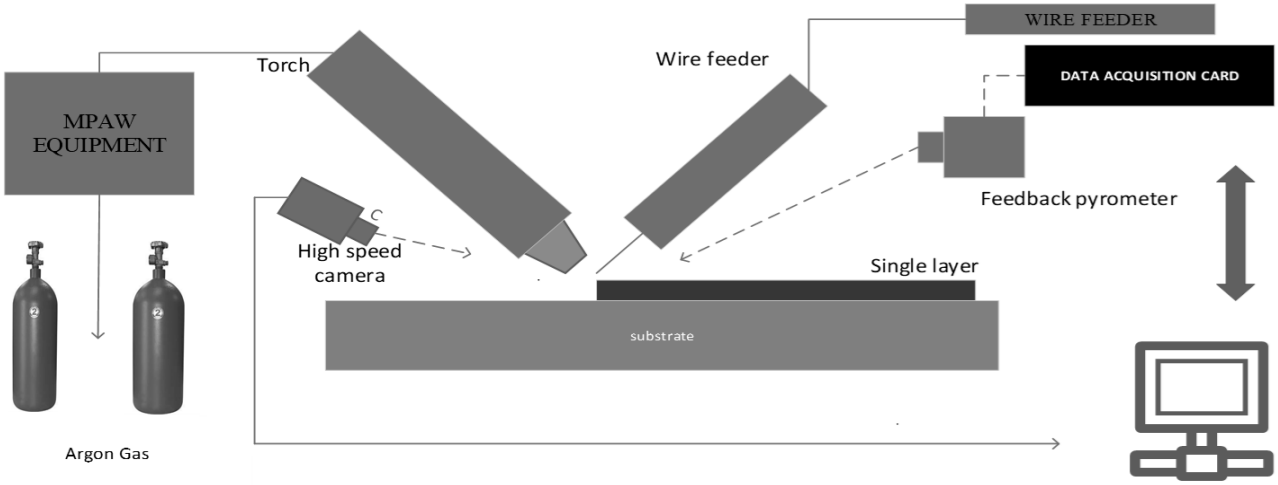

Fig. 3 *Experimental Setup*

For experimental setup, pyrometer is installed to monitor the temperature during single track deposition as shown in Figure 3.10. The same setup is simulated in numerical model where temperature distribution is also monitored. The peak temperature of the experimental single track deposition was verified by comparing it to the corresponding peak simulation temperature. Figure 3.11 displays the results, with the experimental results represented by dashed lines and the simulated outcomes represented by solid lines. The analysis reveals that the simulated findings closely align with the actual measurements in terms of the trend in fluctuations, thereby confirming the accuracy of the FE model.

The maximum temperature obtained in simulation setup is 423 °C and in experiment temperature is 411 °C, with 3 % error. There is slight skewness in the graph where both simulation and experiment setup does not reach maximum temperature at the same time. Simulation setup reach maximum temperature first compared to experimental setup. This occurs because, in the experiment setup, a fraction of the overall arc energy that is absorbed by the work piece is lost due to conduction, while only a small fraction is actually used for melting the filler wire.

The discrepancy between the projected model and experimental results could be attributed to certain assumptions, such as the omission of heat losses from radiation and convection, the assumption of material qualities being independent of temperature, and the ignoring of the impact of viscosity and evaporation on the boundary of the molten pool. The analysis reveals that the simulated findings exhibit a trend of fluctuations that closely aligns with the actual measurements.

The analysis finds that the simulated results display a trend of fluctuations that closely aligns with the actual measurements.

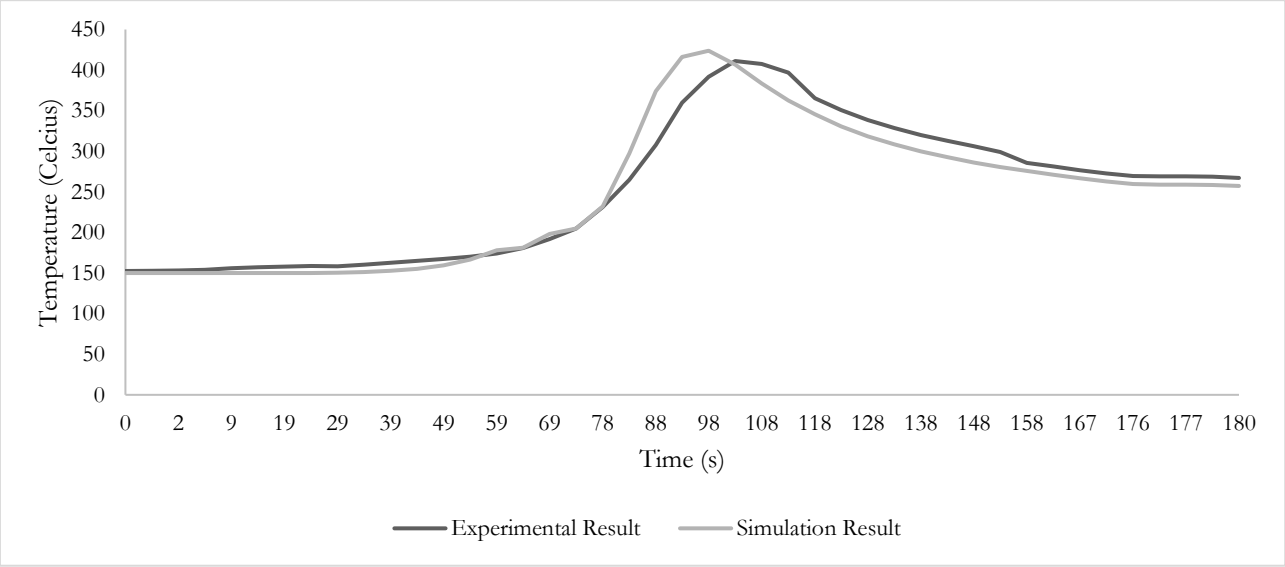

Graph 1 *Graph of the FE Model Validation*

3 Results and Discussion

3.1 Influence of Processing Parameters on Width of Molten Pool (WMP)

At constant current and voltage, melt pool area decreases with increasing scan speed, resulting in a decrease in melt through depth. This decrease in heat input and energy transfer during laser irradiation leads to a decrement in bead dimension. One research reveals that increasing scan speed affects melt pool width and surface roughness [20]. This study confirms the current state of knowledge in the literature by decreasing trend of WMP as shown in Graph 2 (a).

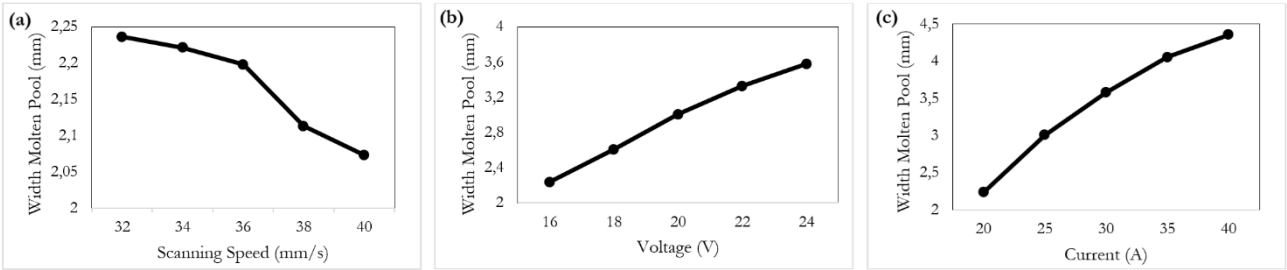

Graph 2 *WMP on different processing parameters (a) Speed at constant 20A and 16V setting (b) Current at constant 32mm/s and 16V setting (c) Voltage at constant 20 A and 16V setting*

WMP increase at higher current level at constant speed and voltage as shown in Graph 2 (b) due to the increasing heat input as the current increases. When welding current is set to its maximum value, the melt pool width will likely be wider at constant speed-voltage setting. This larger and deeper melt pool may result in better bonding and a stronger weld connection. Previous research also explain that melting size increases at higher current levels due to increasing heat input and arc pressure [21]. As the current increases, the energy intake and arc pressure also increase, leading to a larger cavity and molten pool.

Welding voltage increase pulse energy thus increasing heat input. The increases in voltage and power of the arc, along with the power-density distribution, and the magnitude and distribution of forces caused by the arc plasma, would result in an increase in both melt pool temperature and width. The increment of the arc voltage resulted in an increment on the WMP shown in Graph 2 (c) suggests that higher voltage levels generate more heat at the heat source, resulting in a higher melt pool temperature.

3.2 Width of Molten Pool (WMP)

The WMP is measured at the widest length of the ellipsoidal melt pool shape as shown in Fig. 4 below from 30 experimental settings with different combinations of parameters are performed with parameters from Tab. 3. The highest temperature in the legend is 1400 °C, which is stainless steel's melting point.

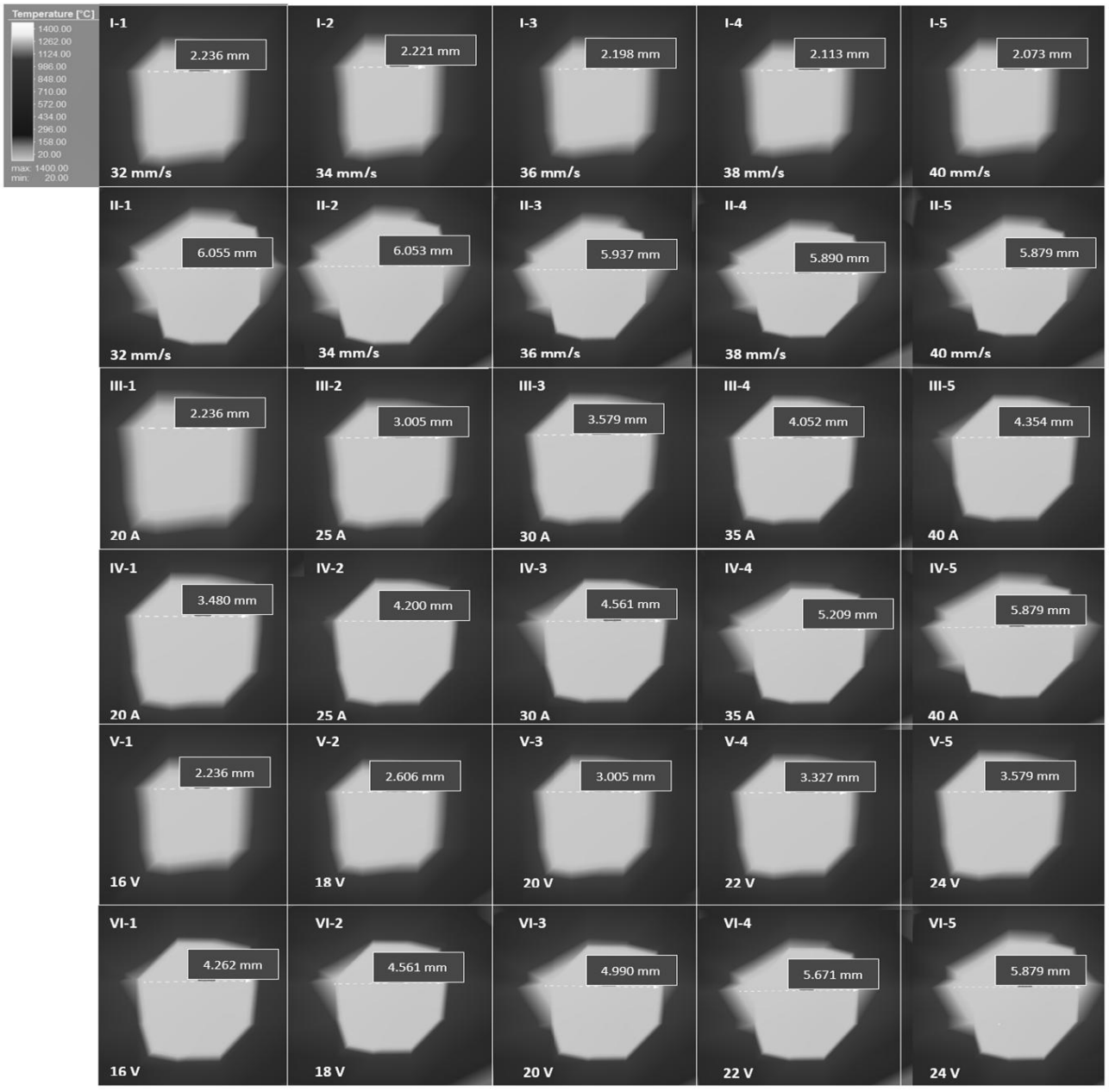

Fig. 4 *WMP under different scan speeds (I, Current = 20A, Voltage = 16V) and (II. Current = 40A, Voltage = 24V), various current (III, Speed = 32mm/s, Voltage = 16V) and (IV, Speed = 40mm/s, Voltage = 24V) and at various voltage (V, Speed = 32mm/s, Current = 20A) and (VI, Speed = 40mm/s, Current = 40A)*

The morphologies of the melt pool are different under different scanning parameters. From the temperature scale, the maximum temperature which is 1400 C in lightest yellow colour is assumed as the melted pool area since the temperature is the melting point of the filler wire (stainless steel material). Previous research reveals that tensile properties of components decline with increasing WMP [22]. Smaller WMP samples exhibit higher strength, while larger WMP samples exhibit lower strength. When melt pool width is small, the feeding wire's diameter is large, causing heat flow to flow downward through the substrate. As WMP increases, the wire's size decreases, allowing more cool wire to be fed into the molten pool.

3.3 Tool Path Planning

This study focus on two tool path planning optimisation which are parallel and zigzag deposition direction throughout the MPWAAM process. The temperature distribution, heat diffusion, temperature gradient, and high-temperature locations are all important aspects to consider during multilayer deposition. The contour graph analysis in Fig. 5 (a) and (b) helps identify workpiece sections experiencing greater or lower temperatures during the deposition process where varying colours reflecting a different temperature range. Warmer colours (yellow and red) are used to indicate hotter places, whereas cooler colours (blue) are used to depict cooler regions.

Fig. 5 *Temperature distribution graph for (a) Parallel and (b) Zigzag toolpath*

Graph 3 and temperature distribution in Fig. 5 shows Zigzag tool path reach higher interpass temperature compared to Parallel tool path. Therefore, it may be inferred that parallel deposition demonstrates better heat diffusion compared to zigzag deposition.

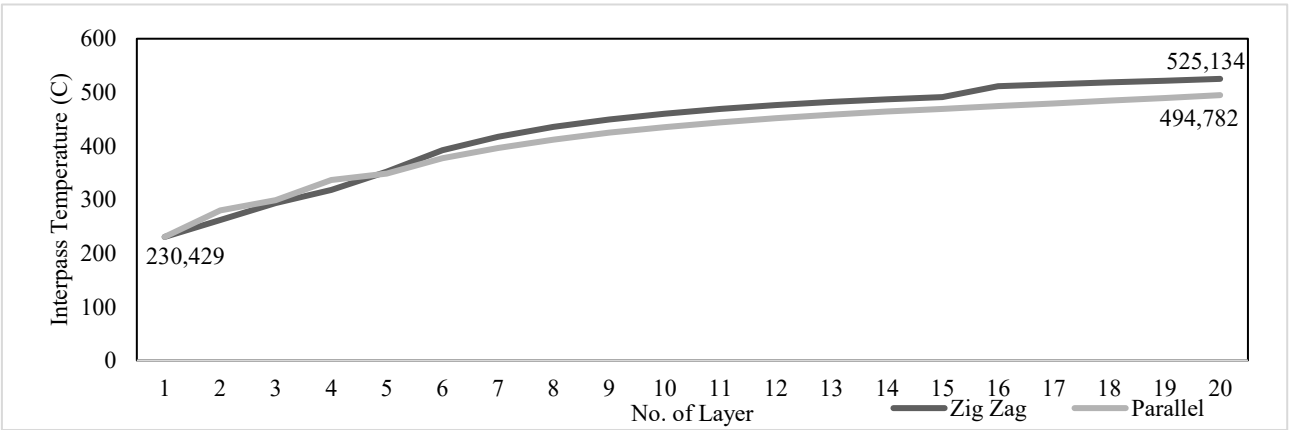

Graph 3 *Multilayer Interpass Temperature for Parallel and Zigzag Tool Path*

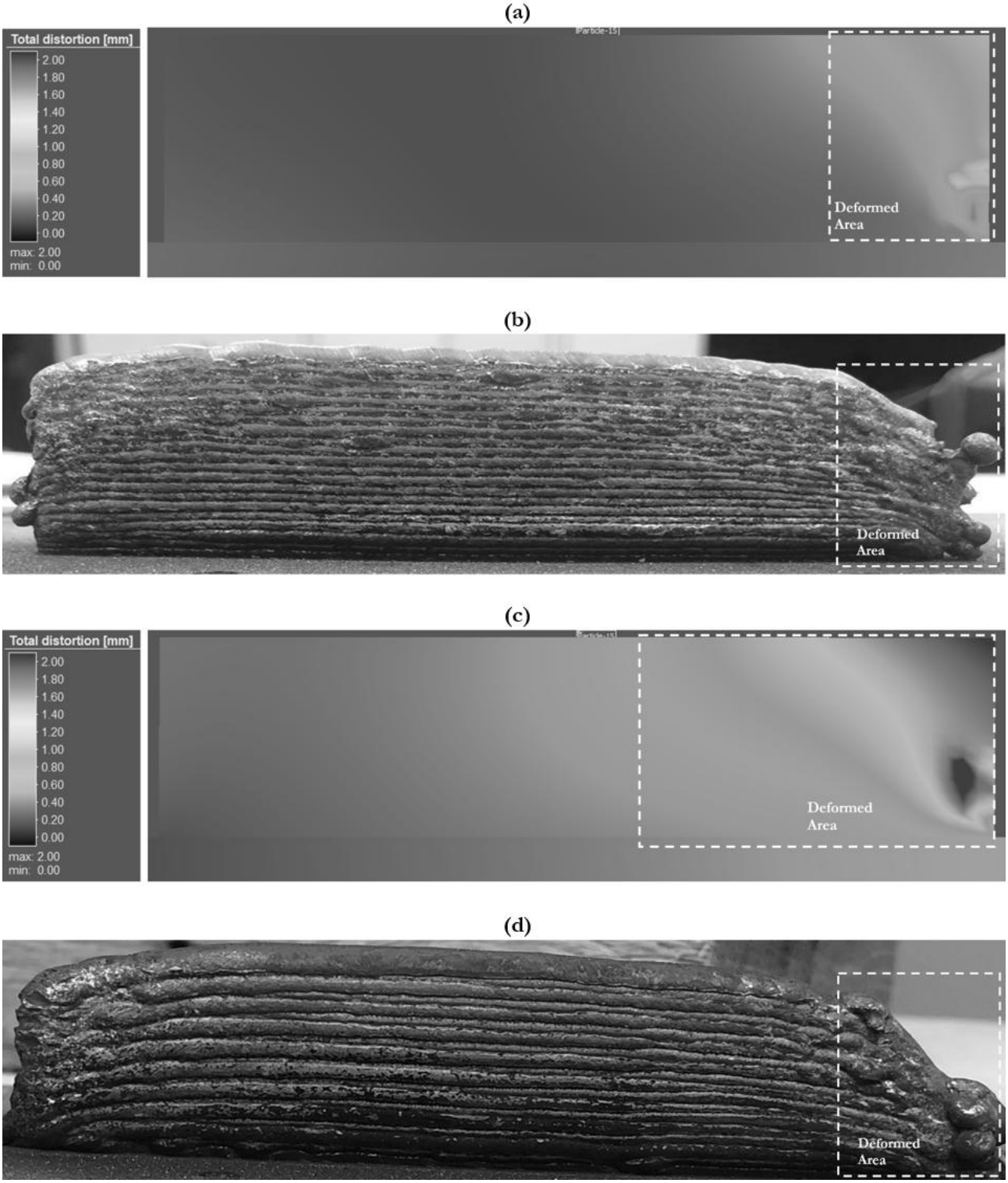

Fig. 6 *Total distortion contour graph for (a) Parallel and (c) Zigzag toolpath and¨final experimental products for (b) Parallel and (d) Zigzag*

The parallel toolpath deposition process as shown in Fig. 6 (a) and (b) show slight distortion at the corner end. This toolpath design features concurrent heating and cooling cycles for each layer, which persist until the final layer is deposited. As the deposition height increases, the high-temperature area of the molten pool gradually expands. The material buildup acts as a thermal insulator that decreasing heat dissipation from the molten pool [23]. Heat accumulation increases in the molten pool zone between previously deposited layers.

As the deposition height increased, there are decrease in heat losses since material buildup functioned as a thermal insulator. This decreasing heat dissipation from the molten pool also cause by convection and radiation [24]. The material from prior layers acts

as a heat sink, allowing additional heat to collect in the current layer's molten pool region.

The zigzag deposition process shown in Fig. 6 (c) and (d) involves depositing material layers in a back-and-forth zigzag pattern, with the micro plasma heat source moving in opposite directions. The high-temperature area of the molten pool expands as more layers are added with shorter interlayer cooling time compared to parallel toolpath. With each new layer added, the portion of the material experiencing high temperatures (in the molten state) expands. The contour graph of Fig. 6 (c) emphasise specific locations with concentrated heat, indicated by small, isolated hot-spots. These localised high-temperature zones impact the final product material's characteristics and cause thermal deformation and residual strains as displayed in Figure 9 (d) with large part distortion. This is supported with previous research that found shorter intervals for cooling between layers lead to elevated temperature levels and substantial modifications in microstructure, in contrast to longer cooling intervals [25].

4 Conclusion

Selecting appropriate welding parameters is crucial for optimal width and fusion in MPWAAM process. The study determines there is an inverse relationship between the scan speed and the width of the molten pool, meaning that as the scan speed increases, the width of the molten pool decreases. This is due to the fact that increased speed results in reduced duration of material interaction time and decreased heat input. The relationship between current and voltage is directly proportional to the amount of heat input. An increase in heat input results in a larger molten pool and higher temperature.

Besides, tool path planning strategy influences the properties and quality of the final product where parallel tool path design with longer interlayer cooling time minimized part distortion and residual stresses. MPWAAM torch in parallel tool path design will return to its original position thus allowing more cooling time for deposited layer before subsequent layer is deposited. The zigzag toolpath deposition approach differs from the parallel toolpath in temperature distribution and heat dispersion parameters, potentially impacting 3D printed components' quality and mechanical qualities.

Acknowledgement

This work is supported by Universiti Teknikal Malaysia Melaka (UTeM) and the Ministry of Higher Education Malaysia (MOHE). This work was financially supported by an MOHE research grant, Fundamental Research Grant Scheme (FRGS) - FRGS/1/2020/TK0/UTEM/02/22.

References

[1] S. MOTADAKA, "A review of 3D printing research from computer and information science perspective: Challenges and research directions," *unpublished*, Aug. 2019.

[2] T. A. RODRIGUES, V. DUARTE, R. M. MIRANDA, T. G. SANTOS, AND J. P. OLIVEIRA, "Current status and perspectives on wire and arc additive manufacturing (WAAM)," *Materials (Basel)*, vol. 12, no. 7, 2019, doi: 10.3390/ma12071121.

[3] S. W. WILLIAMS, F. MARTINA, A. C. ADDISON, J. DING, G. PARDAL, AND P. COLEGROVE, "Wire + Arc additive manufacturing," *Mater. Sci. Technol. (U.K.)*, vol. 32, no. 7, pp. 641–647, 2016, doi: 10.1179/1743284715Y.0000000073.

[4] S. JHAVAR, N. K. JAIN, AND C. P. PAUL, "Development of micro-plasma transferred arc (μ-PTA) wire deposition process for additive layer manufacturing applications," *J. Mater. Process. Technol.*, vol. 214, no. 5, pp. 1102–1110, 2014, doi: 10.1016/j.jmatprotec.2013.12.016.

[5] C. S. WU, L. WANG, W. J. REN, AND X. Y. ZHANG, "Plasma arc welding: Process, sensing, control and modeling," *J. Manuf. Process.*, vol. 16, no. 1, pp. 74–85, 2014, doi: 10.1016/j.jmapro.2013.06.004.

[6] M. S. SAWANT AND N. K. JAIN, "Characteristics of single-track and multi-track depositions of Stellite by micro-plasma transferred arc powder deposition process," *J. Mater. Eng. Perform.*, vol. 26, no. 8, pp. 4029–4039, 2017, doi: 10.1007/s11665-017-2828-y.

[7] J. L. Z. LI, M. R. ALKAHARI, N. A. B. ROSLI, R. HASAN, M. N. SUDIN, AND F. R. RAMLI, "Review of wire arc additive manufacturing for 3D metal printing," *Int. J. Autom. Technol.*, vol. 13, no. 3, pp. 346–353, 2019, doi: 10.20965/ijat.2019.p0346.

[8] M. A. JABBAR, "A design of experiment analysis approach to improve part quality in 3D printing," *Manuf. Technol.*, vol. 23, no. 3, pp. 290–297, 2023, doi: 10.21062/mft.2023.034.

[9] S. H. NIKAM, N. K. JAIN, AND S. JHAVAR, "Thermal modeling of geometry of single-track deposition in micro-plasma transferred arc deposition process," *J. Mater. Process. Technol.*, vol. 230, pp. 121–130, 2016, doi: 10.1016/j.jmatprotec.2015.11.022.

[10] J. H. CHUJUTALLI, M. I. LOURENÇO, AND S. F. ESTEFEN, "Methodology for the

determination of heat source parameters for a FCAW process," in *Proc. 13th Int. Symp. Pract. Des. Ships Other Float. Struct. (PRADS)*, 2016.

[11] M. MATUŠ et al., "Geometric accuracy of components manufactured by SLS technology regarding the orientation of the model during 3D printing," *Manuf. Technol.*, vol. 23, no. 2, pp. 233–240, 2023, doi: 10.21062/mft.2023.027.

[12] J. JIANG AND Y. MA, "Path planning strategies to optimize accuracy, quality, build time and material use in AM—A review," *Micromachines*, vol. 11, no. 7, p. 633, 2020, doi: 10.3390/mi11070633.

[13] F. MICHEL, H. LOCKETT, J. DING, F. MARTINA, G. MARINELLI, AND S. WILLIAMS, "A modular path planning solution for wire + arc additive manufacturing," *Robot. Comput. Integr. Manuf.*, vol. 60, pp. 1–11, 2019, doi: 10.1016/j.rcim.2019.05.009.

[14] R. B. DINWIDDIE, R. MANNELLO, AND H. MICROMET, "Thermal conductivity 26, thermal expansion 14," in *Proc. 26th Int. Thermal Conductivity Conf. and 14th Int. Thermal Expansion Symp.*, 2001.

[15] J. GOLDAK, M. BIBBY, J. MOORE, R. HOUSE, AND B. PATEL, "Computer modeling of heat flow in welds," *Metall. Trans. B*, vol. 17, no. 3, pp. 587–600, 1986, doi: 10.1007/BF02670226.

[16] P. V. SENTHIIL AND A. SHIRRUSHTI, "Finite element simulation of plasma transferred ARC welding [PTAW] of structural steel," *J. Eng. Res. Appl.*, vol. 4, no. 10, pp. 6–11, 2014.

[17] U. PRISCO, "Shape of the melt pool produced by a moving Gaussian heat source," *Weld. World*, vol. 65, no. 11, pp. 2105–2118, 2021, doi: 10.1007/s40194-021-01167-3.

[18] S. KOU, *Welding Metallurgy*, 2nd ed. Hoboken, NJ, USA: John Wiley & Sons, 2003, doi: 10.22486/iwj.v4i3.150243.

[19] R. K. ROY, *Design of Experiments Using the Taguchi Approach: 16 Steps to Product and Process Improvement*, New York, NY, USA: Wiley-Interscience, 2001. [Online]. Available: https://books.google.com.my/books?id=6zq3c3FaCq8C

[20] N. A. ROSLI, M. R. ALKAHARI, F. R. RAMLI, M. F. BIN ABDOLLAH, S. I. A. KUDUS, AND S. G. HERAWAN, "Parametric optimisation of micro plasma welding for wire arc additive manufacturing by response surface methodology," *Manuf. Technol.*, vol. 22, no. 1, pp. 59–70, 2022, doi: 10.21062/mft.2022.001.

[21] N. MURUGAN AND V. GUNARAJ, "Prediction and control of weld bead geometry and shape relationships in submerged arc welding of pipes," *J. Mater. Process. Technol.*, vol. 168, no. 3, pp. 478–487, Oct. 2005, doi: 10.1016/j.jmatprotec.2005.03.001.

[22] Q. WU et al., "Effect of molten pool size on microstructure and tensile properties of wire arc additive manufacturing of Ti-6Al-4V alloy," *Materials (Basel)*, vol. 10, no. 7, 2017, doi: 10.3390/ma10070749.

[23] F. SIKAN, P. WANJARA, J. GHOLIPOUR, A. KUMAR, AND M. BROCHU, "Thermomechanical modeling of wire-fed electron beam additive manufacturing," *Materials (Basel)*, vol. 14, no. 4, pp. 1–21, 2021, doi: 10.3390/ma14040911.

[24] D. JAFARI, T. H. J. VANEKER, AND I. GIBSON, "Wire and arc additive manufacturing: Opportunities and challenges to control the quality and accuracy of manufactured parts," *Mater. Des.*, vol. 202, p. 109471, 2021, doi: 10.1016/j.matdes.2021.109471.

[25] L. COSTA, R. VILAR, T. RETI, AND A. M. DEUS, "Rapid tooling by laser powder deposition: Process simulation using finite element analysis," *Acta Mater.*, vol. 53, no. 14, pp. 3987–3999, 2005, doi: 10.1016/j.actamat.2005.05.003.